

# Ammonia at Blodgett Forest, Sierra Nevada, USA

M. L. Fischer and D. Littlejohn

Environmental Energy Technologies Division, E.O. Lawrence Berkeley National Laboratory, 1 Cyclotron Rd., Berkeley CA, 94720, USA

Received: 5 September 2007 – Accepted: 27 September 2007 – Published: 5 October 2007

Correspondence to: M. L. Fischer (mlfischer@lbl.gov)

14139

## Abstract

Ammonia is a reactive trace gas that is emitted in large quantities by animal agriculture and other sources in California, which subsequently forms aerosol particulate matter, potentially affecting visibility, climate, and human health. We performed initial measurements of  $\text{NH}_3$  at the Blodgett Forest Research Station (BFRS) during a two week study in June, 2006. The site is used for ongoing air quality research and is a relatively low-background site in the foothills of the Sierra Nevada. Measured  $\text{NH}_3$  mixing ratios were quite low ( $<1$  to  $\sim 2$  ppb), contrasting with typical conditions in many parts of the Central Valley. Eddy covariance measurements showed  $\text{NH}_3$  fluxes that scaled with measured  $\text{NH}_3$  mixing ratio and calculated aerodynamic deposition velocity, suggesting dry deposition is a significant loss mechanism for atmospheric  $\text{NH}_3$  at BFRS. A simple model of  $\text{NH}_3$  transport to the site supports the hypothesis that  $\text{NH}_3$  is transported from the Valley to BFRS, but deposits on vegetation during the summer. Further work is necessary to determine whether the results obtained in this study can be generalized to other seasons.

## 1 Introduction

In California and the nation, many areas are out of compliance with federal particulate matter standards designed to protect human health (NRC 1998; NRC 2000). Nationally, Congress has set a goal to remediate current and prevent future impairment of visibility in over 150 federally designated Class 1 Federal (Malm et al., 2000) designated sites. Ammonia ( $\text{NH}_3$ ) is the primary gas to form aerosols in combination with acidic species (e.g.,  $\text{SO}_x$ ,  $\text{NO}_x$ ) that are produced in combustion processes from energy related activities. While mixing ratios of combustion derived species are regulated,  $\text{NH}_3$  is not. If ammonia limits aerosol concentrations, then controls on emissions of  $\text{NO}_x$  and perhaps  $\text{SO}_x$  may not be effective in controlling aerosol concentrations, visibility, or protecting human health.

14140

The magnitude of  $\text{NH}_3$  fluxes are expected to vary enormously over space.  $\text{NH}_3$  is emitted from strong point sources (e.g. animal agriculture), medium strength distributed sources (e.g., fertilized fields and automobile catalytic converters), and exchanged with spatially vast areas of soil and vegetation (Potter et al., 2001; Kirchstetter et al., 2002; Battye et al., 2003). Ammonia is of particular interest in California because it is emitted in large amounts from agricultural sources in the Central Valley, leading to high (20–40 ppb) surface layer  $\text{NH}_3$  mixing ratios (Fischer et al., 2003; Lunden et al., 2003; Chow et al., 2006). For example, recent work suggest that San Joaquin Valley area emissions might range from 8 to 42  $\text{g N ha}^{-1} \text{day}^{-1}$  (11 to 50  $\text{ng NH}_3 \text{ m}^{-2} \text{ s}^{-1}$ ) in winter and summer respectively, with approximately 78 % of the summertime emissions derived from animal agriculture (Battye et al., 2003).

While most  $\text{NH}_3$  measurements have been made in urban areas in California, some measurements have been made in rural settings. Airborne measurements in the afternoon mixed layer showed that ammonium compounds (i.e.,  $\text{NH}_3 + \text{NH}_4^+$ ) were the dominant component of the N budget with variable  $\text{NH}_3$  concentrations corresponding to mixing ratios of  $10 \pm 7$  and  $2.5 \pm 0.5$  ppb in boundary layer above the foothills of the Sierra in the boundary layer above Lake Tahoe respectively (Zhang et al., 2002). In contrast, a ground-based study at Lake Tahoe measured significantly lower concentrations corresponding to approximate mixing ratios between 0.6 to 1.5 ppb and mean summer deposition rates between 3 to 11  $\text{ng N m}^{-2} \text{ s}^{-1}$  (Tarnay et al., 2001). The previous work raises the question of whether there are vertical gradients in  $\text{NH}_3$  caused by dry deposition or whether the differences in  $\text{NH}_3$  at the surface and aloft are due to different measurement times.

Here we describe a short term study of the  $\text{NH}_3$  mixing ratios and  $\text{NH}_3$  fluxes at a rural site in the foothills of the Sierra Nevada.

14141

## 2 Methods

The methods section includes a description of the measurement site, the fast response  $\text{NH}_3$  instrument, the methods used for data reduction, a filter sampling system used to provide comparative  $\text{NH}_3$  measurements, a method used to calculate the aerodynamic deposition velocity expected under different meteorological conditions, and a predictive model for  $\text{NH}_3$  mixing ratios at the measurement site.

### 2.1 Measurement Site

#### 2.1.1 UC Berkeley Blodgett Forest Research Station

We measured  $\text{NH}_3$  mixing ratios and fluxes near the University of California's Sierra Nevada the Blodgett Forest Research Station (BFRS), located west of the Sacramento region as shown in Fig. 1. The BFRS site is an attractive site for this work because it is representative of large areas of forested land with acidic soils in the mountainous Western US and has been the site of ongoing air quality measurements (Goldstein et al., 2000; Dillon et al., 2002; Kurpius et al., 2002; Farmer et al., 2006). Although recent work at BFRS has studied mixing ratios and fluxes of several reactive nitrogen species,  $\text{NH}_3$  has not been measured previously.

The BFRS tower is located at  $38.88^\circ \text{N}$ ,  $120.62^\circ \text{W}$ , at an elevation of 1315 m in a re-growing ponderosa pine plantation. Tree heights ranged from approximately 8–10 m. Terrain is gently sloping downward from east to west. Power to the site is provided by a diesel generator located approximately 130 m due north of the tower site. The predominant winds are upslope from the southwest during the day and downslope from the northeast during the night.

### 2.2 $\text{NH}_3$ instrument

Ammonia was measured using a sensitive fast-response quantum-cascade laser (QCL) spectrometer operating at a frequency of  $965 \text{ cm}^{-1}$  (Aerodyne Research Inc

14142

(ARI), similar to that used for eddy covariance flux measurements of NO<sub>2</sub> (Zahniser 2003; Horii et al., 2004). The precision of the NH<sub>3</sub> instrument is normally 0.3 ppb (1 sigma) for data collected at a frequency of 10 Hz. The instrument provided highly automated control of high frequency data collection, zero adjustments, and zero and span checks as described below using a dedicated software package (TDLWintel).

In addition to the QCL spectrometer, additional data was collected. First, a sonic anemometer (Gill Windmaster Pro) was used to measure fluctuations in virtual air temperature and 3-D winds. The digital output from the anemometer was logged by the computer controlling the QCL spectrometer. The anemometer was physically positioned so that the sensing volume was located 30 cm from the inlet manifold of the NH<sub>3</sub> instrument. Second, a data logger (Campbell CR23X) recorded gas flow rates controlled by mass flow controllers, inlet surface temperatures measured with thermocouples, atmospheric temperature and relative humidity (Vaisala Y45), and short wave solar radiation (Kipp and Zonen CM3).

The NH<sub>3</sub> and ancillary meteorological measurements were made at a height of approximately 10 m above the ground, sufficient to reach slightly above the nearby vegetation. The combined weight of the spectrometer, support electronics and thermal control system and liquid nitrogen storage dewar for automated refills of the spectrometer detector dewar (total of ~200 kg) required a platform scissor-lift. The scissor lift was located at a distance of approximately 8 m from the main BFRS meteorological tower. During the two day period from 24 to 25 July, when the LBNL measurements were compared with the filter sampler, the platform was lowered to a height of ~6 m to match the height of the filter sampler. The filter sampler was deployed on the main BFRS tower.

To achieve high temporal resolution necessary for eddy covariance measurements, we designed a high flow rate gas sampling and calibration subsystem that transmits ambient NH<sub>3</sub> vapor to the spectrometer with minimal residence time. A schematic of the inlet and calibration system is shown in Fig. 2. A flow of ambient air is drawn into the sample manifold by the combination of a manifold flow pump (at 20 slpm) and

14143

into the NH<sub>3</sub> spectrometer at a rate (approximately 25 slpm) determined by the pump speed (Varian 600 dry scroll) and the diameter of a critical orifice inlet. After entering the critical orifice (which reduces the pressure to approximately 50 Torr), air is passed through a 0.2 micron PTFE air filter (Gelman PALL, Acro-50), a 2 m long 1 cm diameter PFA Teflon tube to the multipass optical cell contained within the QCL spectrometer. All glass surfaces are siloxyl coated (General Electric) and surfaces are heated as suggested in Neuman et al. (1999). In our application, the temperatures of the different inlet parts were maintained between 40 and 45°C by a set of four temperature control circuits, while the optical bench including the optical absorption cell was maintained at 30°C.

During the measurements, the instrument zero was adjusted every 30 min, under control of the spectrometer computer, by overfilling the inlet manifold with an approximately 60 slpm flow of dry nitrogen supplied by a large liquid N<sub>2</sub> supply dewar. Typically, zero adjustments were significantly less than 1 ppb. In addition, the instrument zero and span were checked periodically. Zeros were generally checked every 30 min. The span of the instrument was checked by reversing a backflow of 300 sccm that normally removes a 100 sccm flow of NH<sub>3</sub> supplied from a permeation tube source. After applying NH<sub>3</sub> for 30 s, the backflow is reestablished removing NH<sub>3</sub> from the inlet. The response time of the instrument to an approximately 15 ppb step in NH<sub>3</sub> mixing ratio was checked once each hour by applying a NH<sub>3</sub> from a permeation tube source to the N<sub>2</sub> flow. As shown in Fig. 3, the response is well characterized by the sum of exponential decay terms as

$$\text{NH}_3(t) = \text{No}(a_1 \exp(-t/\tau_1) + a_2 \exp(-t/\tau_2)), \quad (1)$$

where  $a_1 = 0.8 \pm 0.05$ ,  $\tau_1 = 0.35 \pm 0.05$  s,  $a_2 = (1-a_1)$ , and  $\tau_2 = 4 \pm 1$  s. The uncertainties in the values reported for the decay coefficients time constants represent variations in the best fit values obtained from fits taken over the experimental period.

14144

### 2.3 Data reduction

The 10 Hz data  $\text{NH}_3$  were processed to estimate mean  $\text{NH}_3$  mixing ratios and  $\text{NH}_3$  fluxes. For mean  $\text{NH}_3$ , a continuous estimate of instrument zero was estimated as a spline interpolation of  $\text{NH}_3$  values obtained during the stable period at the end of zero checks (see Fig. 3). The instrument zero was less than 1 ppb for 90% of the data, until 21 June, when the instrument ran out of cryogenics. Upon restarting the instrument on 23 June, the instrument noise level had increased by nearly an order of magnitude (to  $\sim 3$  ppb in 1 s integration), leading to a larger variation in zero level. Following subtraction of instrument zeros, mean mixing ratios were calculated for 1 and 12 h bins.

$\text{NH}_3$  flux was computed for 1/2 h intervals from the covariance of the 10 Hz  $\text{NH}_3$  mixing ratios and the vertical wind using standard techniques (Baldocchi et al., 1988). Wind fields were rotated to a coordinate system with zero mean vertical wind. Fluctuations in ammonia,  $\text{NH}_3'$ , virtual temperature,  $T'$ , and wind vectors,  $u'$ ,  $v'$ , and  $w'$ , were calculated by subtracting 1/2 hour block averages. Vertical fluxes were calculated as the covariance between vertical wind fluctuations,  $w'$ , and other quantities. Periods during  $\text{NH}_3$  zero or span measurements were excluded. The mean ammonia flux,  $F_{\text{NH}_3} = \langle w' \text{NH}_3' \rangle$  was estimated 1/2 h interval. The time lag between  $w'$  and  $\text{NH}_3'$ , required to maximize  $F_{\text{NH}_3}$ , was determined from lag correlation plots. Typical values for the best lag were small ( $< 0.3$  s), and roughly consistent with that expected from the measured step response of the inlet system.

To correct for loss of high frequency  $\text{NH}_3$  fluctuations due to finite frequency response of the gas inlet, we applied an empirically derived multiplicative correction (Horii et al., 2004). The correction was computed from the measurements of sensible heat obtained from the sonic anemometer. Here sensible heat is calculated as,  $H = \rho C_p \langle w' T' \rangle$ , where  $\rho$  and  $C_p$  are the density and specific heat of air respectively. We calculated the correction factor,

$$f_{\text{corr}} = w' T' / w' T'_{\text{sm}}, \quad (2)$$

14145

where  $T'_{\text{sm}}$ , is obtained by convolving  $T'$  with the double exponential decay function describing the step response to  $\text{NH}_3$  span decay in Eq. (1). Typical values for  $F_{\text{corr}}$  ranged from 1 to 1.2 depending on the atmospheric stability, indicating that the  $\text{NH}_3$  captured most of the high frequency fluctuations contributing to the flux. As an additional check of the frequency response, power spectra for  $w' T'$ ,  $w' T'_{\text{sm}}$ , and  $w' \text{NH}_3'$  were computed for 1/2 h periods and compared with the  $-4/3$  power law expected from Komolgorov similarity theory.

We determined whether the  $\text{NH}_3$  fluxes were stationary by comparing the 1/2 h mean flux with the mean of the individual fluxes determined from 5 min sub-intervals. Data was considered to be stationary when the flux calculated from the subintervals is within 30% of the 1/2 h mean flux (Foken et al., 1996). Non-stationary conditions typically occur during periods of intermittent turbulence which typically occurs on nights when the air is stably stratified and friction velocity,  $u^* = \langle -w'u' \rangle^{1/2}$  is low ( $u^* < 0.1 \text{ m s}^{-1}$ ). Non-stationary fluxes of nitrogen oxides have also been observed at BFRS, associated with emissions from the generator (Farmer et al., 2006). We excluded the data ( $\sim 20\%$ ) obtained when the wind direction was within 45 degrees of north.

### 2.4 Filter sampling

Ambient  $\text{NH}_3$  concentrations were determined during a two day period (starting on the evening of 23 June and continuing into midday of 25 June) using filter samples collected with the Desert Research Institutes (DRI) sampler (Chow et al., 1993). As described above, the inlet of the filter sampler was located at a height of 5.5 m off the ground on the main meteorological tower. In this method, two filter samples are collected simultaneously. One filter is exposed to a flow of ambient air, while the other is exposed to air that has had gaseous  $\text{NH}_3$  removed by an annular denuder. Then the denuded filters collected only particulate  $\text{NH}_4^+$ , while the undenuded filter collected both gas and aerosol. Gaseous  $\text{NH}_3$  is estimated as the difference between undenuded and denuded measurements. In this experiment, four sets of paired (denuded

14146

and undenuded) citric acid coated filters were exposed to air flows near 100 liters per minute (measured before and after each sample was collected) over the two day period using 12 h collection times (18:00–06:00 and 06:00–18:00 PDT, or 01:00–13:00 and 13:00–01:00 GMT). Before and after sample collection the filters were stored in capped, bagged, and stored in an ice chest. Following collection on 25 June, the samples were returned to DRI for analysis of  $\text{NH}_4^+$  ions captured on the citric acid.

## 2.5 Estimate of maximum deposition velocity

As a check on the observed  $\text{NH}_3$  fluxes, we computed deposition velocities,  $V_d = F_{\text{NH}_3}/\text{NH}_3$ , for each 1/2 h interval and compared it to a simple model for the maximum deposition velocity expected if all  $\text{NH}_3$  molecules are reaching the leaf surfaces are adsorbed. In general, deposition velocity can be expressed in a resistance based model as,

$$V_d = (R_a + R_b + R_c)^{-1}, \quad (3)$$

where  $R_a$ ,  $R_b$ , and  $R_c$  are the aerodynamic, leaf boundary layer, and stomatal resistances respectively. In the limit that the vegetation is nitrogen limited and readily accepts all  $\text{NH}_3$  reaching the leaf surface,  $R_c$  can be assumed to be small and a maximum deposition velocity can be written as

$$V_{d\text{max}} = (R_a + R_b)^{-1}, \quad (4)$$

Using standard turbulence models for the surface layer fluxes, one can write a set of expressions for  $R_a$  and  $R_b$  (Wesely 1989; Horii et al., 2004). Here

$$R_a = u/u_*^2 - \chi_H/(ku_*), \quad (5)$$

where  $k$  is the Von Karmen coefficient ( $\sim 0.4$ ). Under stable conditions  $\chi_H$  can be expressed as

$$\chi_H = 5(z - d)/L, \quad (6)$$

14147

where  $z$  is the measurement height,  $d$  is the displacement height (often assumed to be 0.75 vegetation height), and  $L$  is the Monin–Obukhov length scale,  $L = -kg\langle w'T' \rangle / Tu_*^3$ , and  $g$  is the acceleration due to Earth's gravity. Stable conditions are defined as when  $L > 0$ . Under unstable conditions ( $L < 0$ ),

$$\chi_H = \exp(0.598 + 0.39 * \ln(-(z - d)/L) - 0.09 * (\ln(-(z - d)/L))^2). \quad (7)$$

Finally, the boundary layer resistance at the leaf surface can be written as

$$R_b^{-1} \sim u^*/7.1 \quad (8)$$

Under the conditions observed at a mixed deciduous forest in Northeastern United States, Horri et al. (2004) observed  $0.01 < V_d < 0.08 \text{ ms}^{-1}$ .

## 2.6 Simulation of $\text{NH}_3$ mixing ratios

Measured  $\text{NH}_3$  mixing ratios were compared with simulated  $\text{NH}_3$  concentrations derived from and a regional emission inventory estimate of  $\text{NH}_3$  emissions combined with a particle back trajectory calculation of time and space specific surface influence on atmospheric gas concentrations and dry deposition of  $\text{NH}_3$ .

A simple  $\text{NH}_3$  emission model was used for these simulations.  $\text{NH}_3$  emissions for June were estimated assuming that cows in dairies and feedlots generated a large fraction of the emissions in the Central Valley. The spatial distribution of cows was obtained from county level statistics for 2002 animal stocking density reported by the United States Department of Agriculture's National Agricultural Statistics Service (NASS, 2004). We estimated the  $\text{NH}_3$  emission factors for the summer conditions by scaling the annual averaged emissions factors by the ratio (2.3) of summer time animal fluxes to annually averaged animal fluxes in the San Joaquin Valley (Battye et al., 2003). The resulting emissions factors are 185 and 64 g  $\text{NH}_3$  animal<sup>-1</sup> day<sup>-1</sup> for dairy and non-dairy cattle respectively. County level  $\text{NH}_3$  fluxes were calculated as the total  $\text{NH}_3$  emissions for each county normalized by the area and are shown in Table 1.

14148

Fluxes from Nevada were set equal to the  $2 \text{ ng m}^{-2} \text{ s}^{-1}$ , similar to low emission counties in California. We did not attempt to include other sources of  $\text{NH}_3$  emission (e.g, other animal agriculture or automobiles) and hence this estimate likely represents a lower limit to  $\text{NH}_3$  fluxes. However, we consider this simple model roughly sufficient for determining the temporal variations in  $\text{NH}_3$  expected at BFRS, particularly given the additional approximations we make in estimating the transport of  $\text{NH}_3$  from remote locations to the site.

The surface influence functions were calculated using the stochastic time inverted Lagrangian transport (STILT) model (Lin et al., 2003). STILT was originally derived from the NOAA HYSPLIT particle transport model (Draxler et al., 1998) for inverse model estimates of surface  $\text{CO}_2$  fluxes (Lin et al., 2004). In our simulations, ensembles of 100 particles were released from the tower site every 2 h and run backward in time for a period of 12 h, which generally allowed the particles to reach locations in the central valley. STILT was driven with NOAA reanalysis meteorology (EDAS40) with 40 km spatial resolution and hourly temporal resolution. Land surface contributions to atmospheric  $\text{NH}_3$  were assumed to be proportional to the time a particle spends within the surface boundary layer.  $\text{NH}_3$  deposition was assumed to depend on the rate of vertical mixing in the atmosphere and parameterized as a residence time  $\tau = z/V_{d0}$ , where  $z$  is the particle altitude above ground and  $V_{d0} = 0.02 \text{ m s}^{-1}$  is an assumed mean deposition velocity. For each time step,  $\Delta t$ ,  $\text{NH}_3$  is updated as

$$\text{NH}_3(t + \Delta t) = \text{NH}_3(t) e^{-\Delta t / \tau} F_{\text{NH}_3} \Delta t / z_i \nu, \quad (9)$$

where  $F_{\text{NH}_3}$  ( $\text{nmol m}^{-2} \text{ s}^{-1}$ ) is the surface  $\text{NH}_3$  flux at the position of the particle,  $z_i$  is the height of the boundary layer, and  $\nu$  is the molecular density of air. Simulations were run both with and without the deposition loss term to estimate the concentration expected for a non-reacting gas.

14149

### 3 Results and discussion

#### 3.1 Surface $\text{NH}_3$ mixing ratios

Figure 4 shows the hourly averages of measured  $\text{NH}_3$  from the LBNL laser spectrometer and the mean results from the 12 h samples collected by the DRI filter system. Both LBNL and DRI data show that  $\text{NH}_3$  was generally between 0 and 2 ppb, with a few periods of higher mixing ratios. Near 13 June, a synoptic event introduced cooler air from the north with lower temperatures and mild precipitation, reducing  $\text{NH}_3$  concentrations significantly. The averages of the LBNL measurements were lower than the filter samples on 24 June, and similar to or higher than the filter samples on 25 June (see Table 2). Inspection of the LBNL data suggests that a significant fraction of the data was noisy and did not pass quality control criteria (~50% in some of the 12 h periods), perhaps causing the poor correlation between LBNL averages and the DRI filter measurements.

We also examined the diurnal variations in  $\text{NH}_3$ . As shown in Fig. 5, there was a significant diurnal cycle with lower mixing ratios at night and higher mixing ratios during the day. This is consistent with having predominantly downslope winds carrying  $\text{NH}_3$  free air from the Sierra Nevada during the night and upslope winds carrying air with  $\text{NH}_3$  from the Central Valley during the day (Dillon et al. 2002).

#### 3.2 Calculated aerosol – gas equilibrium

We considered whether the low  $\text{NH}_3$  mixing ratios might limit ammonium-based aerosol concentrations by comparing measured  $\text{NH}_3$  with previously measured  $\text{HNO}_3$  and the aerosol-gas equilibrium coefficient,  $K_p$ , which defines the minimum  $\text{NH}_3 \cdot \text{HNO}_3$  product required to form  $\text{NH}_4\text{NO}_3$  aerosol (Stelson et al., 1982). Figure 6 shows that  $K_p \gg 1 \text{ ppb}^2$  for most of the observation period. Earlier work at Blodgett showed that  $\text{HNO}_3$  mixing ratios fell in a range of 0.3 to 1.5 ppb (5%–95%) for June–October (Murphy et al., 2006). Assuming a nominal value of 1 ppb  $\text{HNO}_3$ , the minimum  $\text{NH}_3$  mixing

14150

ratio required to support aerosol  $\text{NH}_3 \cdot \text{HNO}_3$  in equilibrium with gas phase constituents is numerically equal to the value of  $K_p$ . Since the measured  $\text{NH}_3$  mixing ratio is generally significantly less than  $K_p$ , this suggests that aerosol  $\text{NH}_3 \cdot \text{HNO}_3$  will not be present in equilibrium with gases. We also note that although  $K_p$  was low during points earlier in June, there were also light rains, which would likely strip  $\text{NH}_3$ ,  $\text{HNO}_3$ , and aerosols from ambient air.

### 3.3 $\text{NH}_3$ Fluctuations, Fluxes, and Deposition Velocities

Before computing  $\text{NH}_3$  fluxes, we examined the power spectra for temporal variations in  $w'T'$ ,  $w'T'_{sm}$ , and  $w'\text{NH}_3$  for each 1/2 h period over which  $\text{NH}_3$  fluxes were calculated. By comparing the spectra of  $w'T'$  and  $w'T'_{sm}$ , we can visually inspect the loss of high frequency power in  $w'T'$  introduced by smoothing  $T'$  with the finite frequency response of the  $\text{NH}_3$  inlet system. A representative set of power spectra are shown in Fig. 7. As expected, the spectra for  $w'T'$  and  $w'T'_{sm}$  are similar, consistent with the smoothing reducing  $w'T'$  by a small amount, and suggesting that  $\text{NH}_3$  fluxes can be accurately recovered. We also note parenthetically that the high frequency slope of all three of the spectra was not as steep as that expected for turbulence in a Komolgorov similarity theory, as observed by other researchers at this and other sites (Farmer et al., 2006).

The  $\text{NH}_3$  fluxes calculated from the 10 Hz data are shown in Fig. 8. Most of the  $\text{NH}_3$  fluxes were small ( $\sim 10 \text{ ng NH}_3 \text{ m}^{-2} \text{ s}^{-1}$ ) or negative. During a several day period early in the campaign when  $\text{NH}_3$  mixing ratios were highest, large negative fluxes ( $-30 \text{ ng NH}_3 \text{ m}^{-2} \text{ s}^{-1}$ ) were observed, indicating that  $\text{NH}_3$  was being lost to the canopy by dry deposition. The mean flux during the measurement period was  $9.2 \pm 1.1 \text{ ng NH}_3 \text{ m}^{-2} \text{ s}^{-1}$ . As a check of whether the estimated fluxes were realistic, we calculated deposition velocities for a subset of the measured fluxes. The subset was obtained by requiring that the  $\text{NH}_3$  mixing was known to better than 50% (at 68% confidence). As shown in Fig. 9, the measured deposition velocities are all less than the maximum deposition velocity estimated from the measured turbulence conditions using Eq. (8),

14151

with a typical ratio for the measured to maximum deposition velocity of approximately 0.5. This is consistent with some combination of imperfect sticking to leaf surfaces and stomatal resistance to  $\text{NH}_3$  uptake by the leaves.

### 3.4 Transport model estimates of $\text{NH}_3$ concentrations

The map of the estimated surface  $\text{NH}_3$  fluxes from cattle is shown in Fig. 10. Surface fluxes range over several orders of magnitude, reflecting the strong emissions from the Central Valley and low emissions from the mountainous regions of the Sierra Nevada. Figure 10 includes an example ensemble of 12-h particle back-trajectories representing a measurement at BFRS at 13:00 h local time on 12 June 2006. This example shows that some particle tracks sweep backward into the Central Valley where they come into contact with high surface  $\text{NH}_3$  fluxes. The predicted  $\text{NH}_3$  concentrations from the back trajectory simulations are compared with measured  $\text{NH}_3$  in Fig. 11. Measured  $\text{NH}_3$  is generally a factor of  $\sim 2$  higher than  $\text{NH}_3$  predicted with deposition and a factor of  $\sim 2$  less than  $\text{NH}_3$  predicted without deposition. The temporal variations in predicted and measured  $\text{NH}_3$  mixing ratios match reasonably well. This is likely because the large variations are caused by variations in the amount of air reaching BFRS from areas in the Central Valley where  $\text{NH}_3$  fluxes are highest.

## 4 Conclusions

We performed an exploratory study of  $\text{NH}_3$  mixing ratios and fluxes at Blodgett Forest during June, 2006. The 1 h averaged  $\text{NH}_3$  mixing ratios ranged from non-detection ( $< 0.2 \text{ ppb}$ ) to about 2 ppb, typical of a low-background site removed from significant sources. The diurnal variations were consistent with upslope flows bringing air with higher  $\text{NH}_3$  to the site during the day. The observed  $\text{NH}_3$  mixing ratios were not sufficient to support  $\text{NH}_4\text{NO}_3$  aerosol in equilibrium with gas phase  $\text{NH}_3$  assuming  $\text{HNO}_3$  was similar to that observed at the site previously.  $\text{NH}_3$  fluxes, measured using the

14152

eddy covariance method, were generally small or negative, consistent dry deposition to the vegetation and no significant net emission. Calculated deposition velocities were generally about half of the maximum expected for deposition to a canopy with aerodynamic and leaf boundary layer resistance but no resistance to leaf uptake (perfect sticking to leaves). This is not surprising given the nitrogen poor soils in the Sierra foothills. Last, we predicted  $\text{NH}_3$  at BFRS by combining a simple  $\text{NH}_3$  emission inventory that considered only emissions from cows (dairy and meat) with a particle back-trajectory model. Measured and predicted  $\text{NH}_3$  concentrations showed substantially similar temporal patterns over synoptic time periods. Predictions with and without  $\text{NH}_3$  deposition bracketed the measured  $\text{NH}_3$  mixing ratios. On the basis of these measurements, we conclude that  $\text{NH}_3$  from the Central Valley had a small but measurable effect on  $\text{NH}_3$  mixing ratios at the BFRS site during the short period of this study, but further measurements would be necessary to determine the whether the same patterns prevail over longer periods, particularly between different seasons.

*Acknowledgements.* We acknowledge B. Duncan, D. Dibartolomeo, and J. Hatch for assistance in construction of the instrument packaging and thermal control systems, M. Zahniser and D. Nelson for technical advice on the use of the  $\text{NH}_3$  spectrometer. A. Goldstein generously shared the research infrastructure at BFRS, while D. and S. Rambeau provided invaluable assistance with arrangements for field work at BFRS. S. Kohl of the Desert Research Institute prepared the filter sampler and performed the analysis of the integrated  $\text{NH}_3$  mixing ratios. J. Lin generously provided the STILT model for the atmospheric transport simulations. The NOAA Air Resources Laboratory (ARL) provided the assimilated meteorology used to drive STILT. N. Brown, R. Cohen, D. Farmer, M. Gallagher, A. Lashgari, M. Lunden and T. Ryerson provided valuable advice and discussion. This work was supported by the California Air Resources Board and by the Laboratory Directors Research and Development Program at the Lawrence Berkeley National Laboratory.

14153

## References

- Baldocchi, D. D., Hicks, B. B. and Meyers, T. P.: Measuring Biosphere-Atmosphere Exchanges of Biologically Related Gases with Micrometeorological Methods, *Ecology* (Tempe) 69(5), 1331–1340, 1988.
- Battye, W., Aneja, V. P., and Roelle, P. A.: Evaluation and improvement of ammonia emissions inventories, *Atmos. Environ.*, 37(27), 3873–3883, 2003.
- Chow, J. C., Chen, L. W. A., Watson, J. G., Lowenthal, D. H., Magliano, K. A. Turkiewicz, K. and Lehrman, D. E.: PM<sub>2.5</sub> chemical composition and spatiotemporal variability during the California Regional PM<sub>10</sub>/PM<sub>2.5</sub> Air Quality Study (CRPAQS), *J. Geophys. Res.-Atmos.*, 111(D10), 2006.
- Chow, J. C., Watson, J. G., Bowen, J. L., Frazier, C. A., Gertler, A. W., Fung, K. K., Landis, D., and Ashbaugh, L. L.: A sampling system for reactive species in the western United States, *Sampling and Analysis of Airborne Pollutants*, Ed. E. D. Winegar and L. H. Keith, New York, Lewis, 209–228, 1993.
- Dillon, M. B., Lamanna, M. S., Schade, G. W., Goldstein, A. H., and Cohen, R. C. Chemical evolution of the Sacramento urban plume: Transport and oxidation, *J. Geophys. Res.-Atmos.*, 107(D5–D6), 4045, 2002.
- Draxler, R. R. and Hess, G. D.: An overview of the HYSPLIT<sub>4</sub> modeling system for trajectories, dispersion, and deposition, *Aust. Meteorol. Mag.*, 47, 295–308, 1998.
- Farmer, D. K., Wooldridge, P. J., and Cohen, R. C.: Application of thermal-dissociation laser induced fluorescence (TD-LIF) to measurement of  $\text{HNO}_3$ , Sigma alkyl nitrates, Sigma peroxy nitrates, and  $\text{NO}_2$  fluxes using eddy covariance, *Atmos. Chem. Phys.*, 6, 3471–3486, 2006.
- Fischer, M. L., Littlejohn, D., Lunden, M. M., and Brown, N. J.: Automated measurements of ammonia and nitric acid in indoor and outdoor air, *Environmental Science & Technology*, 37(10), 2114–2119, 2003.
- Foken, T. and Wichura, B.: Tools for quality assessment of surface-based flux measurements, *Agr. Forest. Meteorol.*, 78(1–2), 83–105, 1996.
- Goldstein, A. H., Hultman, N. E., Fracheboud, J. M., Bauer, M. R., Panek, J. A., Xu, M., Qi, Y., Guenther, A. B., and Baugh, W.: Effects of climate variability on the carbon dioxide, water, and sensible heat fluxes above a ponderosa pine plantation in the Sierra Nevada (CA), *Agricultural & Forest Meteorology*, 101(2–3), 113–129, 2000.
- Horii, C. V., Munger, J. W., Wofsy, S. C., Zahniser, M., Nelson, D. and McManus, J. B.: Fluxes

14154



- of nitrogen oxides over a temperate deciduous forest, *J. Geophys. Res.-Atmos.*, 109(D8), 2004.
- Kirchstetter, T. W., Maser, C. R. and Brown, N. J.: Ammonia emission inventory for the state of Wyoming, Berkeley, CA, E.O. Lawrence Berkeley National Laboratory, 2002.
- 5 Kurpius, M. R., McKay, M., and Goldstein, A. H.: Annual ozone deposition to a Sierra Nevada ponderosa pine plantation, *Atmos. Environ.*, 36(28), 4503–4515, 2002.
- Lin, J. C., Gerbig, C., Wofsy, S. C., Andrews, A. E., Daube, B. C., and Grainger, B. B. S. C. A., Bakwin, P. S., and Hollinger, D. Y.: Measuring Fluxes of Trace Gases at Regional Scales by Lagrangian Observations: Application to the CO<sub>2</sub> Budget and Rectification Airborne (CO-BRA), Study, *J. Geophys. Res.* 109, doi:10.1029/2004JD004754, 2004.
- 10 Lin, J. C., Gerbig, C., Wofsy, S. C., Andrews, A. E., Daube, B. C., Davis, K. J., and Grainger, C. A.: A near-field tool for simulating the upstream influence of atmospheric observations: The Stochastic Time-Inverted Lagrangian Transport (STILT) model - art. no. 4493, *J. Geophys. Res.-Atmos.*, 108(D16), 4493, 2003.
- 15 Lunden, M. M., Revzan, K. L., Thatcher, M. L. F. L., Littlejohn, D., Hering, S. V., and Brown, N. J.: The transformation of outdoor ammonium nitrate aerosols in the indoor environment, *Atmos. Environ.*, 37, 5633–5644, 2003.
- Malm, W. C., Pitchford, M. L., Scruggs, M., Sisler, J. F., Ames, R., Copeland, S., Gebhart, K. A., and Day, D. E.: Spatial and Seasonal Patterns and Temporal Variability of Haze and Its Constituents in the United States, Fort Collins, Cooperative Institute for Research in the Atmosphere, Colorado State University, 2000.
- 20 Murphy, J. G., Day, A., Cleary, P. A., Wooldridge, P. J., and Cohen, R. C.: Observations of the diurnal and seasonal trends in nitrogen oxides in the western Sierra Nevada, *Atmos. Chem. Phys.*, 6, 5321–5338, 2006, <http://www.atmos-chem-phys.net/6/5321/2006/>.
- 25 NRC: Research priorities for airborne particulate matter. I. Immediate priorities and a long-range research portfolio, Washington, DC, National Academy Press, 1998.
- NRC: Research priorities for airborne particulate matter, III. Early Research Progress, Washington, DC, National Academy Press, 2000.
- Potter, C., Krauter, C., and Klooster, S.: Statewide Inventory Estimates Statewide Inventory Estimates of Ammonia Emissions from of Ammonia Emissions from Native Soils and Chemical Native Soils and Chemical Fertilizers in Fertilizers in California, Sacramento, California Air Resources Board, 2001.
- 30 Stelson, A. W. and Seinfeld, J. H.: Relative-Humidity and Temperature-Dependence of the

14155

- Ammonium-Nitrate Dissociation-Constant, *Atmos. Environ.*, 16(5), 983–992, 1982.
- Tarnay, L., Gertler, A. W., Blank, R. R., and Taylor, G. E. Preliminary measurements of summer nitric acid and ammonia concentrations in the Lake Tahoe Basin air-shed: implications for dry deposition of atmospheric nitrogen, *Environ. Pollut.*, 113(2), 145–153, 2001.
- 5 Wesely, M. L.: Parameterization of Surface Resistances to Gaseous Dry Deposition in Regional-Scale Numerical-Models, *Atmos. Environ.*, 23(6), 1293–1304, 1989.
- Zahniser, M. S.: Urban Ammonia Source Characterization Using Infrared Quantum Cascade Laser Spectroscopy, National Atmospheric Deposition Program (NADP) Meeting, Potomac, MD, 2003.
- 10 Zhang, Q., Carroll, J. J., Dixon, A. J., and Anastasio, C.: Aircraft measurements of nitrogen and phosphorus in and around the Lake Tahoe Basin: Implications for possible sources of atmospheric pollutants to Lake Tahoe, *Environmental Science & Technology*, 36(23), 4981–4989, 2002.

14156

**Table 1.** Cattle stocking, area, and estimated NH<sub>3</sub> flux by county.

County	Beef Cows	Dairy Cows	Other Cattle	area (km <sup>2</sup> )	Flux (ng NH <sub>3</sub> m <sup>-2</sup> s <sup>-1</sup> )
Alameda	9401	6	10 405	1888	8
Alpine	1560	0	551	1891	1
Amador	10 112	20	9104	1518	9
Butte	8979	1261	9191	4197	4
Calaveras	14 390	222	12 878	2611	8
Colusa	0	0	7957	2946	2
Contra Costa	0	0	11 596	1843	5
Del Norte	1018	4703	4154	2580	5
El Dorado	4115	9	3551	4390	1
Fresno	23 422	90 550	282 547	15 265	26
Glenn	17 438	17 304	30 655	3366	22
Humboldt	22 333	16 732	24 041	9146	8
Imperial	0	0	386 634	10 687	27
Inyo	0	0	8278	26 120	0
Kern	36 779	74 708	148 553	20 841	14
Kings	5130	138 292	126 108	3561	111
Lake	4764	4	4378	3220	2
Lassen	25 381	38	23 905	11 667	3
Los Angeles	0	0	2092	10 396	0
Madera	15 723	48 086	82 972	5468	32
Marin	9105	10 309	15 998	1331	31
Mariposa	10 204	245	12 130	3715	5
Mendocino	0	0	7691	8983	1
Merced	29 534	223 303	212 270	4937	133
Modoc	41 564	14	33 615	10 097	6
Mono	2989	0	2338	7794	1
Monterey	25 430	1606	46 025	8504	7
Napa	4300	245	3453	1930	3
Nevada	3007	108	1927	2451	2
Orange	392	0	401	2021	0
Placer	0	0	10 004	3595	2
Plumas	5766	7	10 644	6537	2
Riverside	3670	90 359	87 042	18 451	14
Sacramento	16 392	18 337	32 807	2472	31
San Benito	14 408	935	24 054	3556	9
San Bernardino	2918	158 240	110 185	51 334	8
San Diego	6363	5729	13 709	10 752	3
San Francisco	0	0	0	120	0
San Joaquin	19 629	103 534	95 196	3582	86
San Luis Obispo	38 268	550	44 928	8459	7
San Mateo	1474	6	941	1150	2
Santa Barbara	19 482	2669	21 183	7007	5
Santa Clara	0	0	12 692	3304	3
Santa Cruz	984	176	2275	1140	2
Shasta	16 618	562	11 225	9690	2
Sierra	3339	0	3777	2441	2
Siskiyou	34750	1518	28 421	16 094	3
Solano	14 560	3947	26 605	2123	18
Sonoma	14 311	31 986	35 301	4034	26
Stanislaus	42 007	162 878	221 060	3824	142
Sutter	0	0	5321	1543	3
Tehama	29 027	5489	33 679	7555	8
Trinity	2671	12	2252	8137	0
Tulare	31 171	412 462	456 491	12 349	101
Tuolumne	6855	108	5288	5723	2
Ventura	4357	17	4544	4724	1
Yolo	6773	2012	8124	2594	6
Yuba	7419	3325	20 694	1615	17

14157

**Table 2.** Comparison of NH<sub>3</sub> mixing ratios (ppb) from DRI filter samples and averages.

Date time (GMT)	Filter	LBNL
24 Jun 2006 07:00	1.46 (0.05)	0.74 (0.28)
24 Jun 2006 19:00	1.55 (0.05)	0.36 (0.13)
25 Jun 2006 07:00	0.90 (0.12)	0.56 (0.32)
25 Jun 2006 19:00	0.58 (0.14)	0.91 (0.30)

14158



**Fig. 1.** Satellite mosaic image showing the Blodgett Forest Research Station in the forested western foothills of the central Sierra Nevada of California, and the mixed use (agricultural and urban) areas of the nearby Sacramento Valley area.

14159

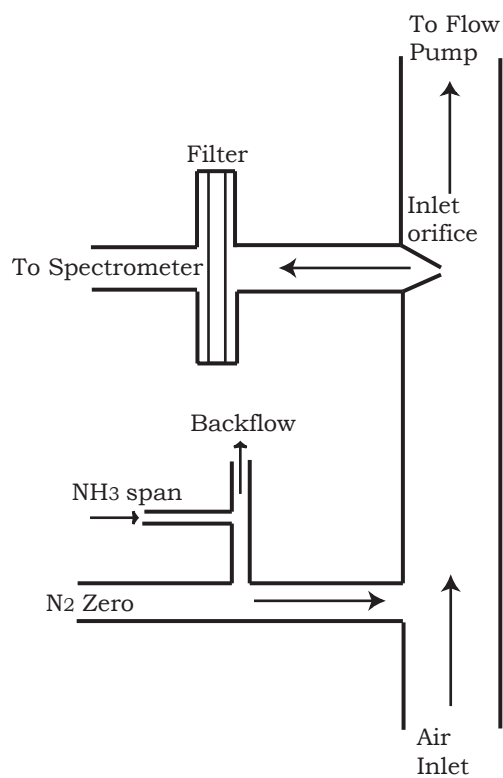


**Fig. 2.** Schematic illustration of the air sampling manifold with critical orifice flow inlet and air filter. Automated instrument zero and span calibrations are performed by periodically flowing  $N_2$  into inlet, either without or with the addition of  $NH_3$  from a permeation tube source.

14160

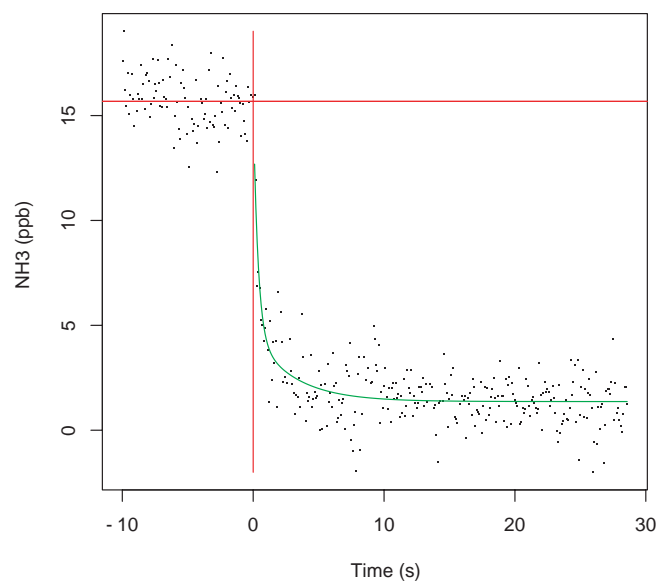


**Fig. 3.** Time series of NH<sub>3</sub> mixing ratio showing transient decay following removal of NH<sub>3</sub> span gas from zero air flow to instrument inlet.

14161

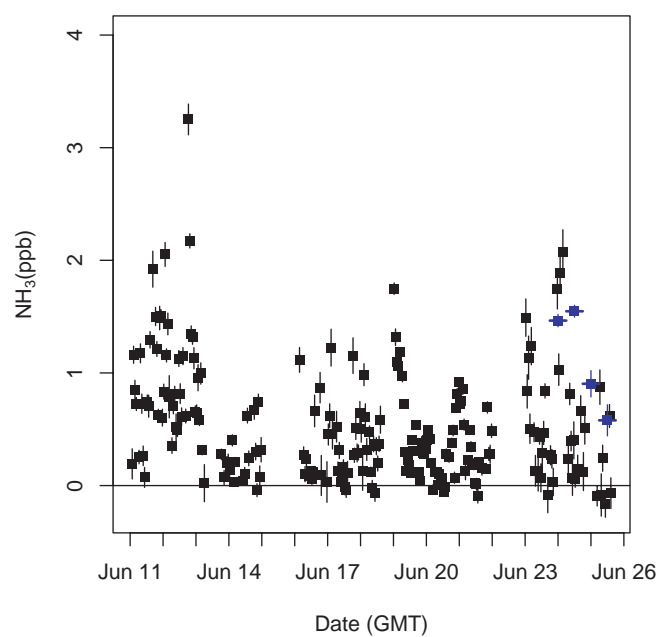


**Fig. 4.** Hourly NH<sub>3</sub> mixing ratios measured at Blodgett Forest in June, 2006. NH<sub>3</sub> data from the laser-spectrometer (black symbols) are averaged into 12 h bins for comparison with integrating filter samples (blue symbols) collected with a sampling system provided by the Desert Research Institute.

14162

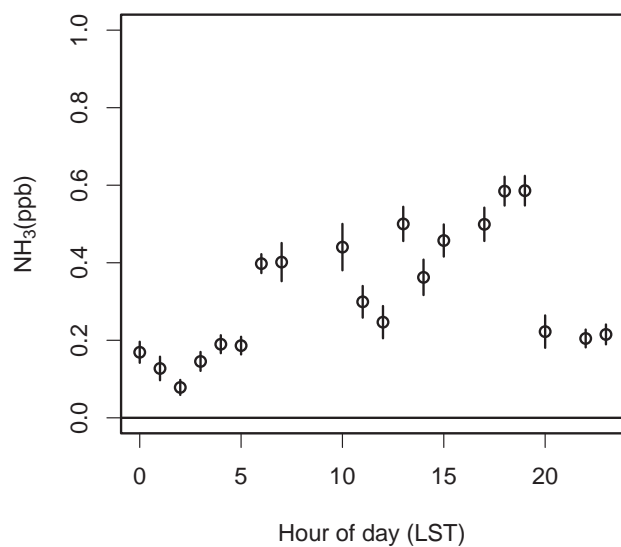


**Fig. 5.** Mean diurnal variation in surface NH<sub>3</sub> mixing ratio from 11 to 26 June 2006.

14163

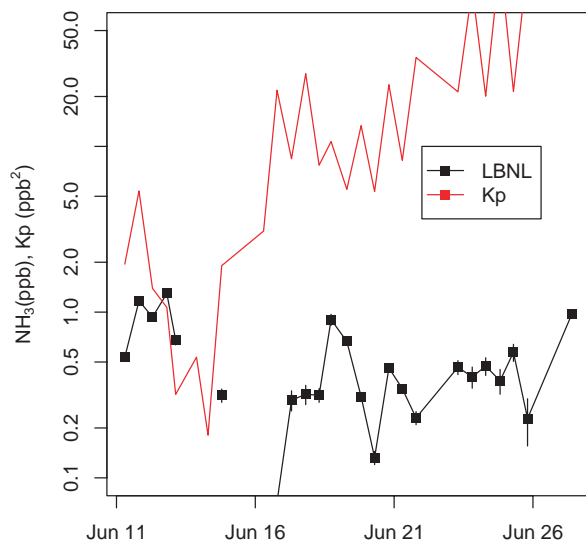


**Fig. 6.** Comparison of NH<sub>3</sub> mixing ratio (black) and aerosol-gas equilibrium partitioning coefficient, Kp (red), indicating minimum product of gas phase NH<sub>3</sub> and HNO<sub>3</sub> mixing ratios necessary for NH<sub>4</sub>NO<sub>3</sub> aerosol to be found in equilibrium with gas phase constituents.

14164

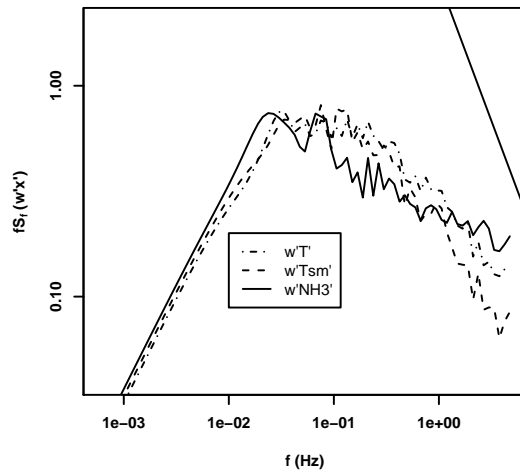


**Fig. 7.** Power spectra of covariance in vertical wind speed with sonic temperature,  $w'T'$ , smoothed sonic temperature,  $w'T_{sm}'$ , and fluctuations in  $NH_3$  mixing ratio,  $w'NH_3'$ . The straight line in upper right shows  $-4/3$  slope expected for fluctuation spectra in an inertial sublayer.

14165

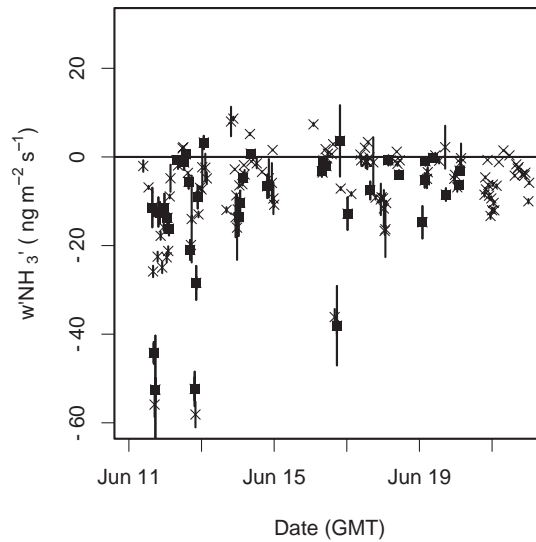


**Fig. 8.** Eddy covariance measurement of  $NH_3$  flux for all time points (crosses) and for those passing quality control criteria for use in calculating deposition velocities (filled squares).

14166

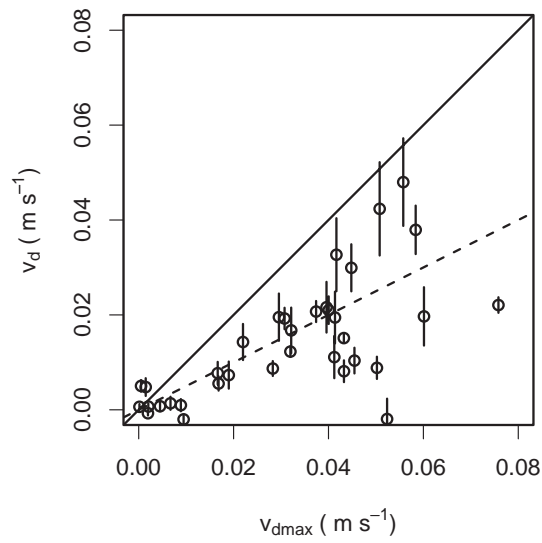


**Fig. 9.** Scatter plot comparison of measured deposition velocity,  $v_d$ , and maximum deposition velocity in the case that all molecules reaching the leaf surface are absorbed,  $v_{dmax}$ .

14167

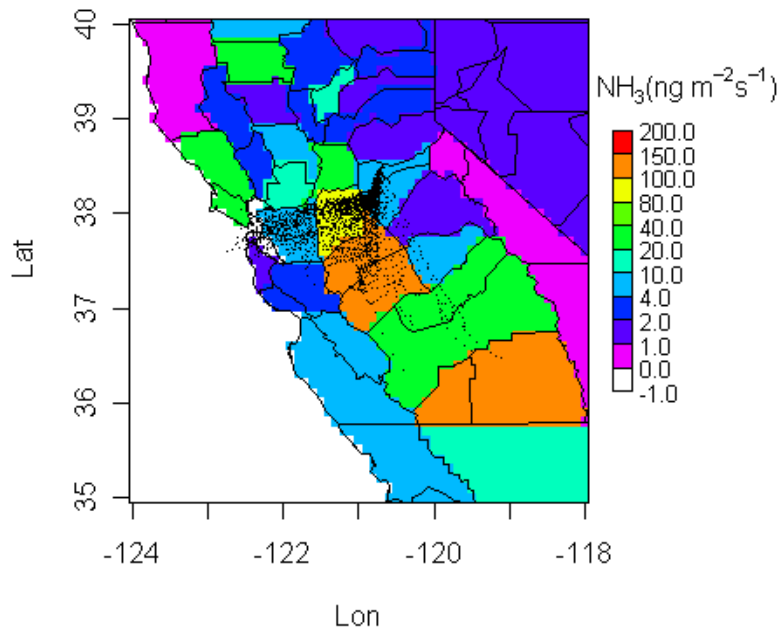


**Fig. 10.** Map of California showing estimated  $\text{NH}_3$  emissions ( $\text{ng NH}_3 \text{ m}^{-2} \text{ s}^{-1}$ ) and an example 12 h back trajectory calculation of showing particles converging at BFRS at midday on 12 June 2006.

14168

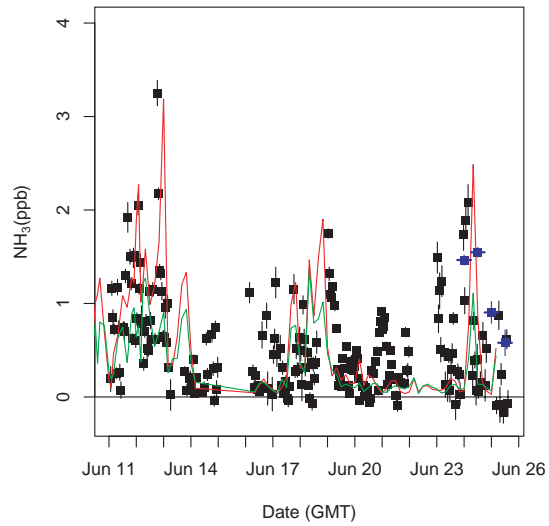


**Fig. 11.** Measured hourly NH<sub>3</sub> mixing ratios from LBNL system (black points), DRI 12 h integrated sampler results (blue points), and predicted NH<sub>3</sub> mixing ratios predicted from the back trajectory calculations and cattle-only NH<sub>3</sub> emission inventory. Predicted NH<sub>3</sub> is scaled to fit on plot so that NH<sub>3</sub> predicted without deposition (red line) is scaled by a factor of 0.5, while NH<sub>3</sub> predicted with deposition (green line) is scaled by a factor of 2.